Aeroacoustics Conferences
20-23 May 2019, Delft, The Netherlands
25th AIAA/CEAS Aeroacoustics Conference

10.2514/6.2019-2546

An investigation of the Mach number dependence of trapped acoustic waves in turbulent jets

Aaron Towne*, Oliver T. Schmidt†, Guillaume A. Brès‡

In addition to the classical Kelvin-Helmholtz modes, compressible jets support hierarchical families of modes that represent upstream and downstream traveling acoustic waves trapped within the jet by its annular shear layer. These trapped waves have recently been shown to participate in a variety of different resonance phenomena, including screech, impingement tones, and a weak subsonic resonance. The properties of the trapped waves vary with the jet Mach number, and recent results from a simple parallel flow vortex sheet model suggest the existence of three distinct Mach number regimes. In this paper, we use a series of large-eddy simulations along with a global linear model to investigate the properties of the trapped waves within and at the boundaries of these different Mach number regimes. We show that the resonance between a pair of duct-like modes predicted by the vortex sheet model for the range $0.82 < M < 1$ persists to lower Mach numbers and is gradually damped away. Moreover, this resonance does not exist at supersonic Mach numbers, and is instead replaced by a weaker interaction between a different pair of trapped waves. We show that a global resolvent-based model provides good approximations of the power spectral density of the trapped waves as a function of both frequency & wavenumber and frequency & streamwise position.

I. Introduction

Turbulent jets support a rich set of waves whose behavior play a central role in the overall dynamics and acoustics of the jet. The most widely studied of these waves are those related to the Kelvin-Helmholtz instability of the shear layer that develops between the jet and the ambient fluid. These waves grow and then decay as they travel downstream, generating a distinctive pattern often refered to as a wavepacket.[1] These wavepackets have been shown to be intimately tied to noise emitted from the jet, especially at downstream angles.

In addition to the downstream-traveling Kelvin-Helmholtz waves, turbulent jets also support hierarchical families of modes representing acoustic waves trapped within the potential core of the jet. These modes were first discovered by Michalke,[2] but were initial disregarded as an unphysical artifact of the local stability analysis performed in that investigation. They were first systematically investigated by Tam & Hu,[3] who postulated that they represent acoustic waves trapped within the potential core by the jet's annular shear layer. They showed that the modes have distinct properties at low subsonic Mach numbers ($M \approx 0.6$) and substantially supersonic Mach numbers ($M \approx 1.5$); while only upstream-traveling trapped waves exist at low Mach numbers, both upstream- and downstream-traveling trapped waves exist at supersonic Mach numbers.

Towne et al.[4] and Schmidt et al.[5] showed that the trapped waves behave differently at high subsonic Mach numbers ($M \approx 0.9$) than they do for the regimes studied by Tam & Hu.[3] Specifically, both upstream- and downstream-traveling trapped acoustic waves exist only within narrow frequency bands. Towne et al.[4] showed that the frequencies at which both types of waves exist changes along the streamwise axis of the jet, which leads to so-called 'turning points' where downstream-traveling waves can be converted into upstream-traveling waves at specific locations within the jet. Coupled with reflection at the nozzle exit plane, this leads to the possibility of resonance between the upstream- and downstream-traveling waves at discrete frequencies,[5] which in turn generates tones that can be observed outside of the jet.

*Assistant Professor, University of Michigan, Ann Arbor, MI, USA
†Assistant Professor, University of California - San Diego, La Jolla, CA, USA
‡Director of Operations; Senior Research Scientist - Aeroacoustics, CASCADE Technologies, Palo Alto, CA, USA

A number of subsequent studies have demonstrated the relevance of the trapped waves in several other resonance phenomena. Jordan et al.[6] found that the trapped waves participate in a resonance with Kelvin-Helmholtz waves that leads to strong tones when a solid edge, such as the flap on a wing, is positioned close to a subsonic jet. Using simulation and experimental data, respectively, Gojan et al.[7] and Edgington-Mitchell et al.[8,9] found evidence that the trapped acoustic waves participate in the resonance leading to screech tones in under-expanded supersonic jets, in line with an earlier conjecture by Shen & Tam.[10] Mancinelli et al[11,12] formulated an improved screech tone prediction model based on these findings. Tam & Ahuja[13] showed that the trapped waves participate in the resonance leading to strong tones in the case of a subsonic jet impinging on an infinte flat plate, and Bogey & Gojon[14] and Jaunet et al.[15] provided additional confirmation of this theory and extended it to supersonic jets.

Given this surge in interest in the trapped acoustic waves, and the different properties observed by Tam & Hu[3] and Towne et al.[4] for different Mach numbers, it is important to gain a complete understanding of the Mach number dependence of these waves. Towne et al.[4] studied their Mach number and temperature ratio dependence using a simple cylindrical vortex sheet model. The model predicted that the properties of the waves observed at Mach 0.9, and the resulting resonance, should be limited to the Mach number range $0.82 < M < 1$ for isothermal jets (for the first family of waves, with slightly different values for other families). Outside of this interval, the properites observed by Tam & Hu[3] are recovered, and the model predicts that these boundaries depend on the jet temperature ratio. Furthermore, the authors speculated that in real jets, the transition between the different behaviors is likely gradual due to the possibility of lightly damped resonance along with ongoing excitation by turbulent fluctuations outside of the high-subsonic range.

While the small number of data points available in the literature were consistent with these model predictions, comprehensive data were not available to confirm the changing properties of the trapped waves as a function of Mach number. This paper will fill in this gap using several large eddy simulations of jets at different Mach numbers as well as global models based on eigenvalue and resolvent analysis of the Navier-Stokes equations linearized about the turbulent mean flow.

The remainder of the paper is organized as follows. Section II reviews the vortex-sheet model and its Mach number predictions. Section III presents the LES setup and results, and section IV introduces the global models and compares them with the LES results. Finally, section V summarizes the paper.

II. Cylindrical vortex sheet model

We begin by reviewing the vortex-sheet model used by Tam & Hu[3] and Towne et al.[4] to describe the trapped waves, with particular focus on the Mach number predictions of the latter authors.

The dispersion relation for a compressible, cylindrical vortex sheet was first derived by Lessen et. al[16] and can be written as

$$\mathcal{D}_j\left(k,\omega;m,M,T\right)=0 \tag{1}$$

with

$$\mathcal{D}_j=\frac{1}{\left(1-\frac{kM}{\omega}\right)^2}+\frac{1}{T}\frac{I_m\left(\frac{\lambda_i}{2}\right)\left[\frac{\lambda_o}{2}K_{m-1}\left(\frac{\lambda_o}{2}\right)+mK_m\left(\frac{\lambda_o}{2}\right)\right]}{K_m\left(\frac{\lambda_o}{2}\right)\left[\frac{\lambda_i}{2}I_{m-1}\left(\frac{\lambda_i}{2}\right)-mI_m\left(\frac{\lambda_i}{2}\right)\right]} \tag{2}$$

and

$$\lambda_i=\sqrt{k^2-\frac{1}{T}\left(\omega-Mk\right)^2}, \tag{3a}$$

$$\lambda_o=\sqrt{k^2-\omega^2}. \tag{3b}$$

I_m and K_m are modified Bessel functions of the first and second kind, respectively. All quantities have been normalized by the jet diameter and far-field thermodynamic quantities such that $M=U_{jet}/c_\infty$ is the acoustic Mach number and $T=T_{jet}/T_\infty$ is the temperature ratio. Equation 1 is satisfied for only certain combinations of the temporal frequency ω and axial wavenumber k, both of which can in general be complex. These special (k,ω) pairs are the eigenvalues of the vortex sheet.

The trapped waves are represented by families of eigenvalues that can be parameterized by the index pair (m,n), where m is the azimuthal wavenumber and n is an effective radial wavenumber related to Bessel function zeros.[4] This can be seen in Figure 1, where the eigenvalues for $St=0.3$, $m=0$, and $M=0.9$ are plotted. The properties of these eigenvalues as a function of frequency, azimuthal wavenumber, Mach

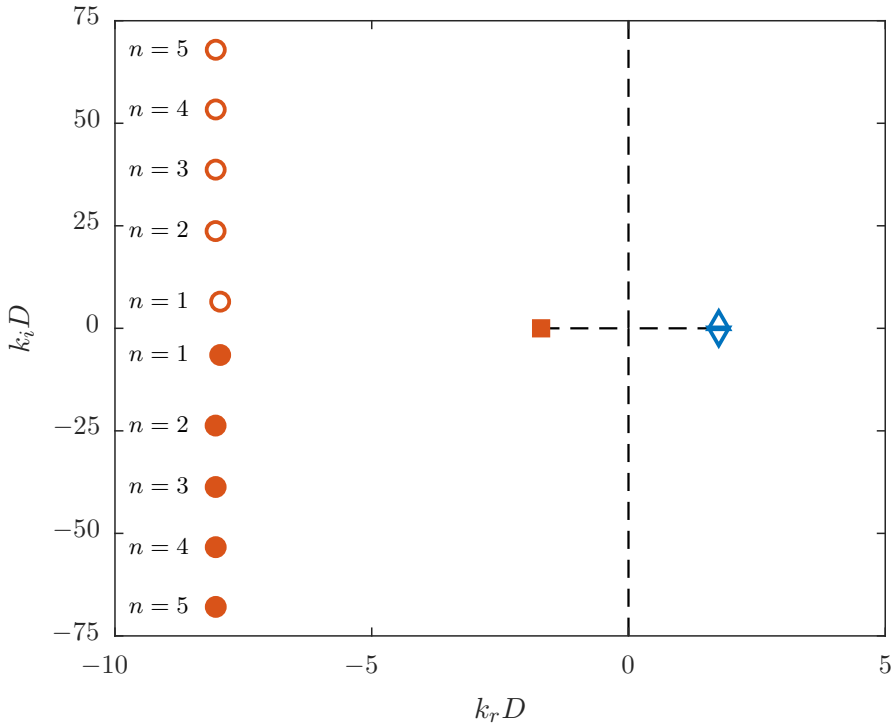

Figure 1: Vortex sheet eigenvalues for $St = 0.3$ and $m = 0$ for Mach number $M = 0.9$: (∇) Kelvin-Helmholtz; (Δ) Kelvin-Helmholtz complex-conjugate; ($\bullet$) upstream duct-like trapped acoustic modes; ($\circ$) downstream duct-like trapped acoustic modes; ($\blacksquare$) discrete free-stream-like acoustic mode. The dashed lines show the continuous branch of eigenvalues for acoustic waves in an unbounded quiescent fluid.

number, and temperature ratio determine the properties of the trapped acoustic waves of interest. In this paper, we will focus on axisymmetric waves ($m = 0$) in isothermal jets ($T = 1$).

Eigenvalue pairs for which both ω and k are real-valued are particularly important as they correspond to *propagating* waves that convect away from their source without growing or decaying. The properties of these propagating waves can be visualized in $k - \omega$ space. Figure 2 shows these dispersion relations for $m = 0$ and $n = 1, 2, 3$ for the three Mach numbers, $M = 0.6, 0.9, 1.5$, which were the focus of Tam & Hu[3] and Towne et al.[4] The Mach number dependence of the trapped waves described in the introduction are apparent. For $M = 0.6$, all of the trapped waves have negative group velocity, $\frac{\partial \omega}{\partial k}$, i.e., they are all upstream-traveling. The other two Mach numbers have waves with both negative and positive group velocities, i.e., there exist both upstream- and downstream-traveling trapped waves. For $M = 1.5$, downstream traveling waves exist at all frequencies, whereas they exist only in limited frequency bands for $M = 0.9$.

Figure 3 shows the dispersion relations for the $(m = 0, n = 1)$ propagating waves for $0.4 < M < 1.5$ at intervals of $\Delta M = 0.04$. It is clear that the three different behavios observed in Figure 2 hold within certain Mach number intervals. Towne et al.[4] showed that the boundaries between the three different behaviors occurs at $M = 0.82$ and $M = 1$.

The resonance observed by Towne et al.[4] and Schmidt et al.[5] at $M = 0.9$ requires the existence of both upstream- and downstream-traveling trapped waves. Thus, the model suggests that resonance should only be possible for $M > 0.82$. However, the interpretation of the model focused exclusively on propagating waves. Weakly damped downstream-traveling waves exist at lower Mach numbers, with the damping increasing with decreasing Mach number. Thus, it is likely that the resonance persists to lower Mach numbers, gradually fading away with decreasing Mach number. We will investigate this possibility using large-eddy simulation and a global linear model.

The model also predicts the possibility of resonance for supersonic Mach numbers. To date, resonance has only been observed in supersonic jets in the case of an obvious downstream end conditions, such as a plate or a shock-cell structure. We will investigate whether an intrinsic resonance occurs in the absence of these end conditions.

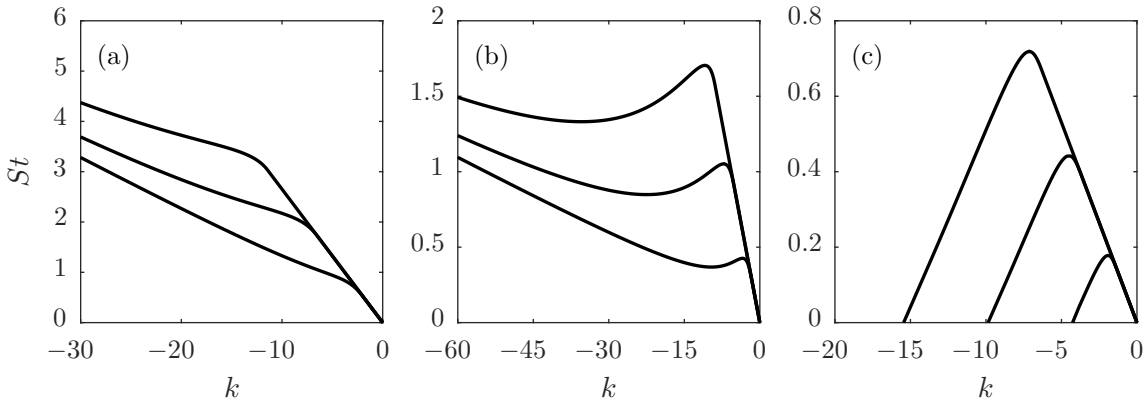

Figure 2: Dispersion relations for the first three $m = 0$ radial modes of the vortex sheet at $T = 1$ and (a) $M = 0.6$; (b) $M = 0.9$; (c) $M = 1.5$.

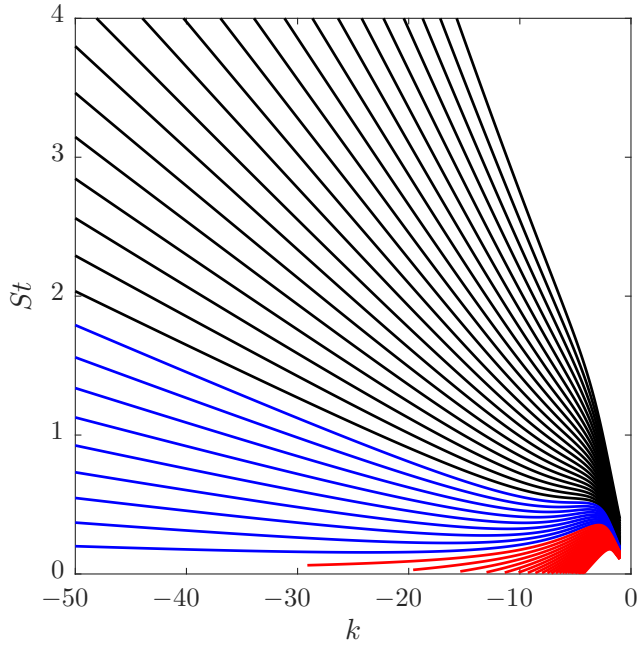

Figure 3: Vortex sheet dispersion relations for the (0,1) family of trapped waves at $T = 1$ and Mach numbers $0.4 < M < 1.5$ with increments $\Delta M = 0.04$. The colors indicate: (black) $M < 0.82$; (blue) $0.82 < M < 1$; (red) $M > 1$.

III. Large-eddy simulation

III.A. LES databases

To explore the Mach number dependence of the trapped waves, large-eddy simulations of isothermal jets issued from a convergent-straight nozzle are performed at five different Mach numbers, $M_j = 0.4, 0.7, 0.8, 0.9$ and 1.5. This Mach number range allows us to examine the behavior of the trapped waves within the low-Mach-number regime, the transition regime around $M = 0.82$, and the supersonic regime. The Reynolds numbers of these jets all fall within the range $Re_j = \rho_j U_j D/\mu_j = [0.3, 1] \times 10^6$, and can thus be considered to be asymptotically high. The flow configuration and operating conditions match companion experiments conducted at the PPRIME Institute, Poitiers, and the $M = 0.9$ and $M = 1.5$ cases have been extensively validated against measurements from these experimentls.[17,18]

The simulations were performed using the compressible flow solver "Charles" developed at Cascade

Technologies, which solves the spatially-filtered compressible Navier-Stokes equations on unstructured grids using a control-volume based finite-volume method.[17] The nozzle geometry is explicitly included in the computational domain and synthetic turbulence boundary conditions are used to model the boundary layer trip present in the companion experiments.[18] To properly capture the internal turbulent boundary layers, localized isotropic mesh refinement and wall modeling[19] are applied on the interior surface from the boundary layer trip to the nozzle exit. This leads to fully turbulent nozzle-exit boundary layers and results in significant improvements for the flow field and sound predictions, compared to those obtained from the typical approach based on a laminar flow assumption in the nozzle. All other solid surfaces are treated as no-slip adiabatic walls. A 1% coflow is imposed outside the nozzle in the simulation to prevent spurious recirculation and facilitate flow entrainment, and sponge layers and damping functions are applied to avoid spurious reflections at the boundary of the computational domain.[20,21] Each of the subsonic simulations was performed on the same adapted grid containing approximately sixteen million grid points and was run for a duration of 2000 acoustic time units (tc_∞/D). The supersonic jet is almost perfectly expanded, and a slightly different setup and parameters were used in this case.[17] The available LES databases consist of time series for the primitive flow variables interpolated onto a structured cylindrical output grid that approximately mirrors the underlying LES resolution.

III.B. Empirical dispersion relations

An empirical dispersion relation for the trapped waves can be obtained from the LES data using the procedure described by Towne et al.[4] and Schmidt et al.[5] Using Fourier transforms in both the streamwise direction and time, the power spectral density is computed as a function of the streamwise wavenumber k and the frequency St. For the subsonic jets, only the first six jet-diameters are included in the streamwise Fourier transform to ensure that the results are dominated by the dynamics within the potential core. For the supersonic jet, we will see shorty that the trapped waves are observed substantially further downstream, so we include data for the first twenty diameters of the jet in this case.

This procedure leads to the frequency-wavenumber diagrams shown in Figure 4 for the five different Mach numbers. Results are shown for pressure at along the jet centerline, which corresponds to the azimuthal mode $m = 0$. Here, iso-contours of the power spectral density of the pressure signal are plotted as a function of the Strouhal number and streamwise wavenumber, which is scaled by the jet diameter. In order to resolve fluctuations occurring at different amplitudes, the scale of the contours is logarithmic and spans four orders of magnitude. The power spectral density at each Mach number if scaled by its maximum value, which is related to the magnitude of Kelvin-Helmholtz wavepackets in the jet. The various bands of energy (the dark regions on the plot) can be interpreted as an "empirical dispersion relation" for the waves within the potential core. The first three vortex sheet dispersion relations ($n = 1, 2, 3$) are shown as dashed lines on top of these empirical dispersion relations.

Focus first on the results for $M = 0.9$ (panel (d)), where the resonance was first observed by Towne et al.[4] and Schmidt et al.[5] The waves predicted by the model are clearly present in the data. Next, consider the results for $M = 0.7$ and 0.8 (panel (b-c)), which are below the theoretical cut-off of $M = 0.82$ for the existence of downstream-traveling waves. Nevertheless, the upstream-traveling waves predicted by the model are clearly present in the data. Moving to the still-lower Mach number of $M = 0.4$ (panel (a)), the waves predicted by the vortex sheet model are no longer present in the data. At the supersonic Mach number $M = 1.5$, the waves predicted by the model are clearly present in the data, and, as expected, the energy is distributed fairly evenly over all frequencies within each family of waves (e.g., $n = 1, 2, 3$). Note that the positive wavenumber trapped modes represent the continuation of the negative wavenumber modes to negative frequencies due to symmetries of the Fourier transform.

III.C. Wavenumber-filtered power spectra

Next, we use the frequency-wavenumber decomposition as a filter to isolate the signature of the trapped and determine their streamwise location. The trapped waves have negative phase-speeds (except for some of the downstream-traveling waves in the supersonic case) while the dominant convective instabilities have positive phase-speeds. Therefore, zeroing the positive wavenumber components and taking an inverse streamwise Fourier transform filters out all waves with positive phase-speeds, effectively distilling the negative phase-speed trapped waves. Contours of the power-spectral-density of the phase-speed-filtered centerline pressure are plotted in Figure 5 for each Mach number. In all cases, the filtered power spectrum is normalized by

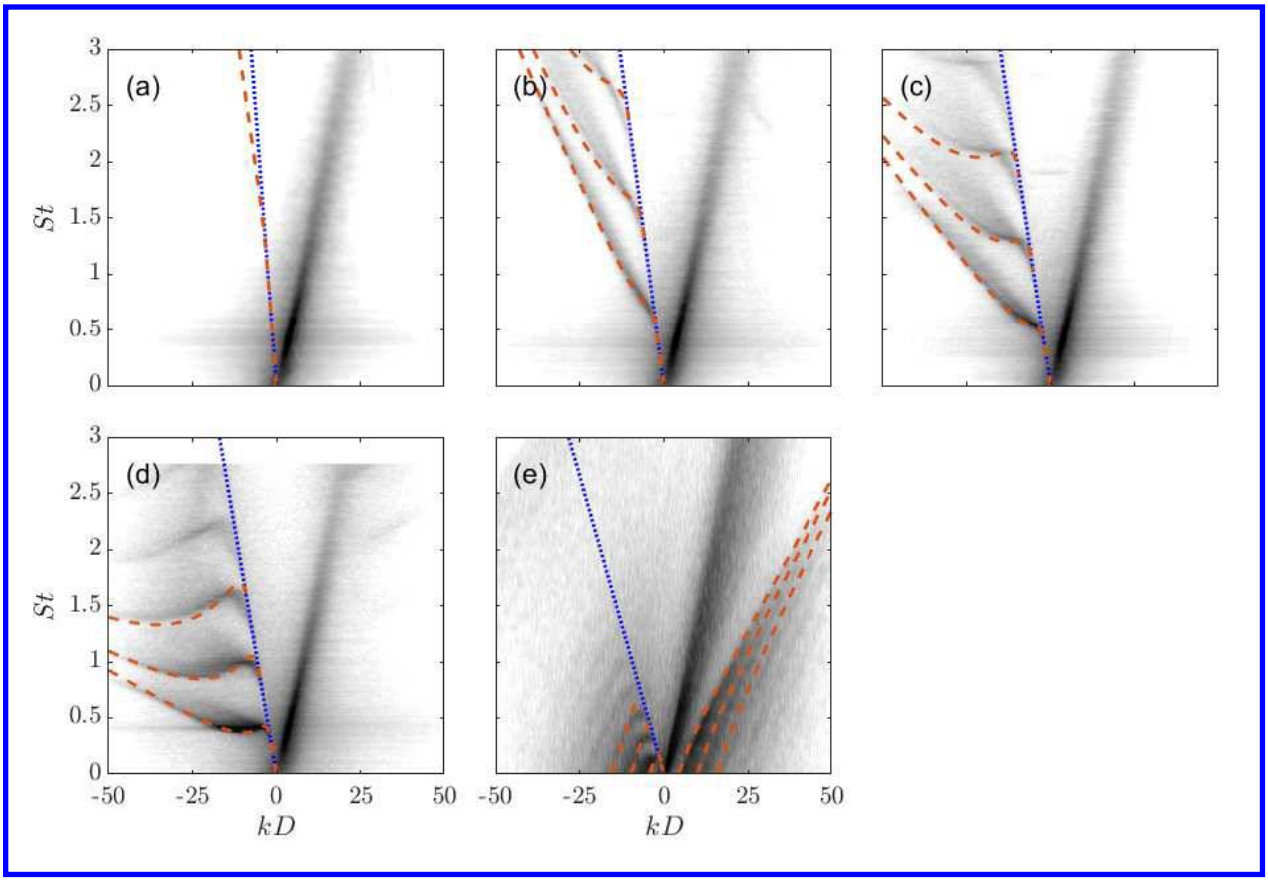

Figure 4: Comparison between modeled and empirical dispersion relations for the $m = 0$ trapped waves in the potential core for (a) $M = 0.4$; (b) $M = 0.7$; (c) $M = 0.8$; (d) $M = 0.9$; (e) $M = 1.5$. Data: (– – –) vortex sheet model; contours show the empirical dispersion relation obtained via frequency-wavenumber decomposition of the pressure along the polar axis.

the maximum amplitude of the unfiltered data, which is again related to the dowstream-traveling Kelvin Helmholtz wavepackets. The contours are distributed logarithmically and span three orders of magnitude. Since only data within the first six diameters of the jet was used for the subsonic cases, no results are available for $x/D > 6$, as indicated by the hashed regions in the figure. Note that the small buildup of energy along the $x/D = 6$ boundary is an artifact of the wavenumber filtering routine.

The filtered power spectral density for $M = 0.9$, shown in Figure 5(d), exhibits a series of distinct high energy regions in $x - St$ space. Towne et al.[4] demonstrated that these energetic regions correspond to trapped acoustic waves that are resonating between the nozzle at $x = 0$ and a downstream end condition provided by turning points created by the slow contraction of the potential core. We see in Figure 5(a-c) that these resonating waves persist to lower Mach numbers below the $M = 0.82$ cutoff predicted by the vortex-sheet model but gradually fade away. The maximum amplitude of the filtered power spectra is an order of magnitude lower for $M = 0.7$ compared to $M = 0.9$, and no trace of the resonating waves remains for $M = 0.4$. These results support the hypothesis of Towne et al.[4] that the resonance observed at $M = 0.9$ will remain active below the $M = 0.82$ cutoff suggested by the vortex sheet model but eventually disappear as the resonance occurs between increasingly damped waves.

The $x - St$ energy distribution is markedly different for the supersonic jet. While there are bands of energy at frequencies associated with the saddle points, substantial energy is also spread over all frequencies. Additionally, the high energy regions extend much further downstream than in the subsonic case, suggesting that the trapped waves persist well beyond the end of the potential core. This suggests a lack of turning points within the potential core that, in the subsonic case, reflect energy back upstream and limit the trapped waves to the first few diameters of the jet.

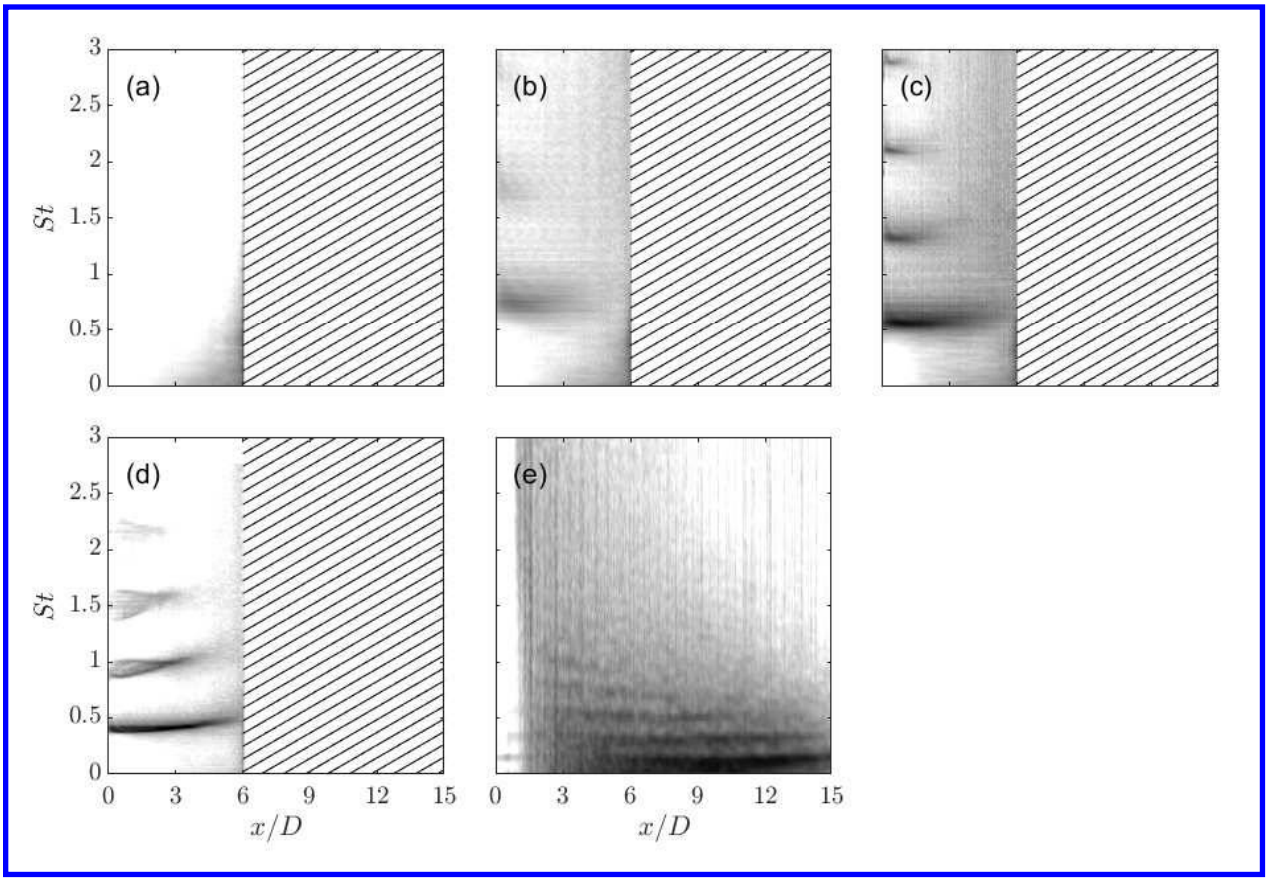

Figure 5: Filtered PSD of the centerline pressure as a function of streamwise position and frequency for (a) $M = 0.4$; (b) $M = 0.7$; (c) $M = 0.8$; (d) $M = 0.9$; (e) $M = 1.5$.

IV. Global linear models

A complete description of the resonance phenomena requires the use of a spatially varying model of the jet in order to capture the end effects needed to convert downstream-traveling waves into upstream-traveling waves. In Towne et al.,[4] a weakly nonparellel model was developed based on the Euler equations linearized about the turbulent mean flow of the jet. Unfortunately, this model is cumbersome for describing the weakly damped waves that are expected to underpin resonance at Mach numbers below 0.82. In the present work, we instead use a global model based on the linearized Navier-Stokes equations using the same numerical framework as in Schmidt et al.[5,22]

IV.A. Theory

Consider the compressible Navier-Stokes equations, which can be written conceptually as

$$\frac{\partial q}{\partial t} = \mathcal{F}(q), \tag{4}$$

where q is a state-vector of flow variables. Applying the Reynolds decomposition

$$q(x, r, \theta, t) = \bar{q}(x, r) + q'(x, r, \theta, t) \tag{5}$$

to equation (4) and isolating the terms that are linear in q' yields an equation of the form

$$\frac{\partial q'}{\partial t} - \mathcal{A}(\bar{q})\, q' = f(\bar{q}, q'), \tag{6}$$

where

$$\mathcal{A}(\bar{q}) = \frac{\partial \mathcal{F}}{\partial q}(\bar{q}) \tag{7}$$

and f contains the remaining nonlinear terms.

Applying Fourier and Laplace transforms to the homogeneous azimuthal and time dimensions, respectively leads to

$$(i\omega I - \mathcal{A}_m)\,\hat{q} = \hat{f}, \tag{8}$$

where $i\omega$ is the Laplace dual of t, m is the azimuthal wavenumber, and $\mathcal{A}_m$ is the operator $\mathcal{A}$ with $\frac{\partial}{\partial\theta}$ replaced by im.

Two different models can be obtained from equation (8) depending on the treatment of ω and $\hat{f}$. The global modes of the flow are obtained by finding special $(\omega, \hat{q})$ pairs for which equation (8) is satisfied with $\hat{f} = 0$. These pairs correspond to eigenvalues and eigenvectors of $\mathcal{A}$. Alternatively, restricting ω for real values and solving equation (8) for $\hat{q}$ gives the input-output relationship

$$\hat{q} = \mathcal{R}\hat{f} \tag{9}$$

defined by the resolvent operator

$$\mathcal{R} = (i\omega I - \mathcal{A}_m)^{-1}. \tag{10}$$

Towne et al.[23] showed that the cross-spectral density tensor $S_{\hat{q}\hat{q}} \triangleq \langle \hat{y}\hat{y}^* \rangle$ can be written in terms of the resolvent operator as

$$S_{\hat{q}\hat{q}} = \mathcal{R} S_{\hat{f}\hat{f}} \mathcal{R}^*, \tag{11}$$

where $\langle\cdot\rangle$ is an ensemble average over different realizations of the jet, $S_{\hat{f}\hat{f}} \triangleq \langle \hat{f}\hat{f}^* \rangle$ is the cross-spectral density of the nonlinear forcing terms, and the asterisk superscript indicates the Hermetian transpose. The forcing cross-spectral density $S_{\hat{f}\hat{f}}$ is in general unknown and is often modeled as unit-amplitude white noise, in which case $S_{\hat{f}\hat{f}} = I$. While deviations from this approximation in the form of correlated nonlinear forcing terms can have important implications,[22] it has been shown to be a reasonable first approximation for turbulent jets.[24] With this approximation, equation (11) becomes

$$S_{\hat{q}\hat{q}} = \mathcal{R}\mathcal{R}^*. \tag{12}$$

This expression can be further simplified by using the singular value decomposition of the resolvent operator,

$$\mathcal{R} = U\Sigma V^*. \tag{13}$$

The singular values, which appear within the diagonal positive-semi-definite matrix Σ, give the square root of the optimal gains between the input and output modes defined by the right and left singular vectors contained in the columns of the orthonormal matrices V and U, respectively. Inserting this decomposition into equation (12) gives

$$S_{\hat{q}\hat{q}} = U\Sigma^2 U^*. \tag{14}$$

Since the right-hand-side of equation (14) will be dominated by terms involving the largest singular values, it can be well-approximated using only the first few singular modes. Finally, the power spectral density is given by the diagonal terms of the approximated $S_{\hat{q}\hat{q}}$ tensor.

IV.B. Global Modes

We begin by examining the global eigenvalue spectra for $m = 0$ and $M = 0.8$, 0.9, and 1.5, shown in Figure 6, which correspond to Mach numbers below, within, and above the range where the vortex sheet model predicts resonance. The eigenvalues for the $M = 0.9$ case, shown in Figure 6(b), were studied in detail by Schmidt et al.[5] They showed that the spectrum is made up of continuous branches and hierarchical families of lightly damped discrete modes. The first family of discrete modes is shown in red in the figure. These modes protrude toward the real axis from a continuous Λ-shaped branch of modes. The discrete modes represent resonating trapped acoustics modes that lie between the two saddle points for the $n = 0$ family of vortex sheet modes, and the additional families of discrete global modes correspond to higher n values.

These discrete modes describing resonance change, but do not disappear, when the Mach number is reduced to 0.8. The global eigenvalue spectrum for this case is shown in Figure 6(a), and the $n = 1$ discrete modes are again shown in red. Instead of protruding from the continuous branch toward the real axis as in the $M = 0.9$ case, the discrete modes now connect two parts of the continuous branch. This is consistent

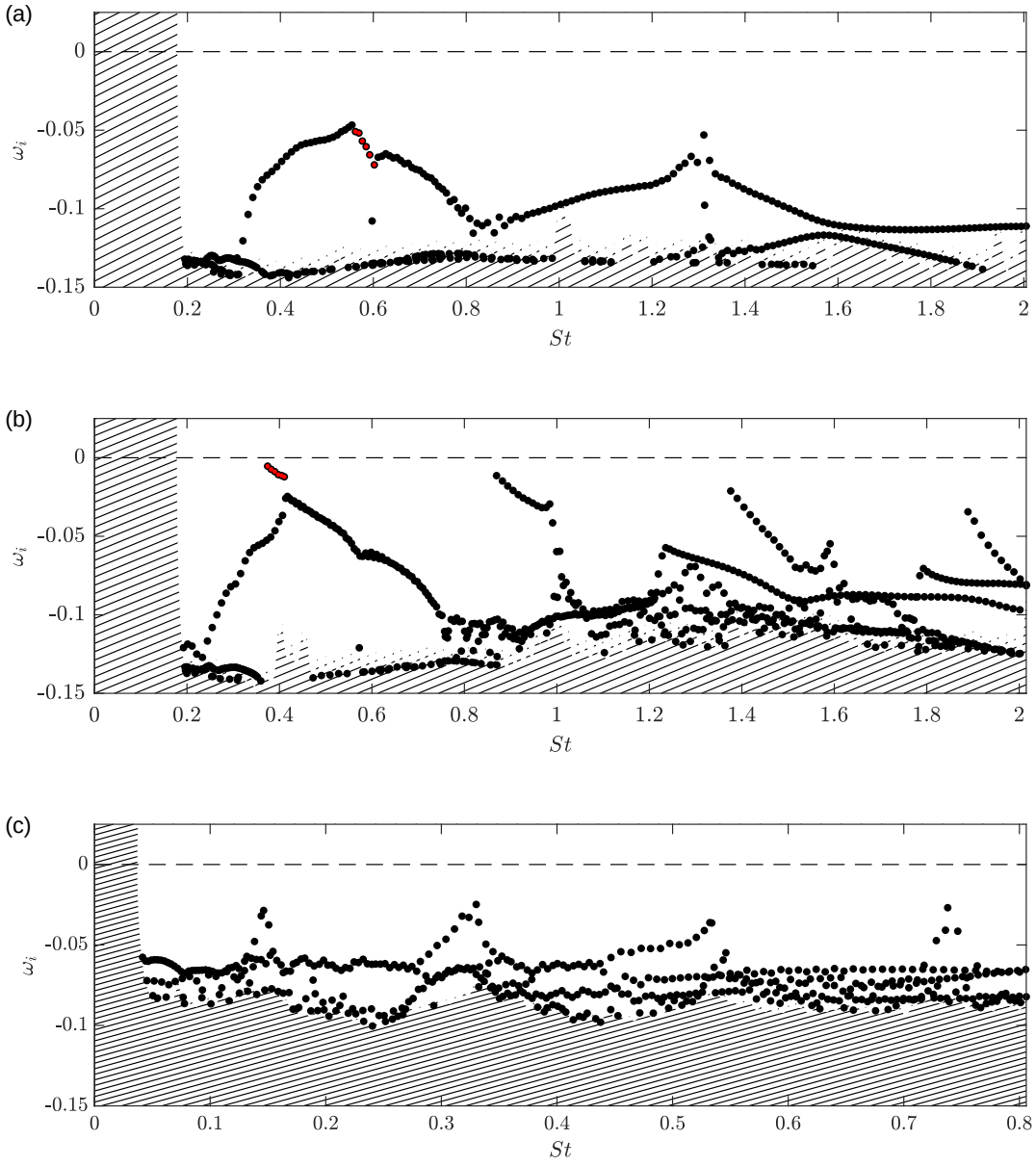

Figure 6: Global eigenvalue spectrum of the jet for: (a) $M = 0.8$; (b) $M = 0.9$; (c) $M = 1.5$.

with the changing shape of the vortex sheet and empirical dispersion relations between the Mach 0.9 and 0.8 cases.

In contrast, no trace of the discrete modes remains in the supersonic case. This is consistent with the properties of the trapped waves. In the $0.82 < M < 1$ range, there exist three types of trapped waves: upstream- and downstream-traveling duct-like modes and an additional upstream-traveling discrete freestream mode.[4] Schmidt et al.[5] found that the discrete modes specifically represent a resonance between the upstream- and downstream-traveling duct-like modes. Towne et al.[4] showed that the upstream-traveling duct-like mode ceases to exist for $M > 1$. As a result, the discrete global modes disappear in the supersonic case. However, there remain Λ-shaped peaks in the continuous spectra, akin to the structure of the continuous branch in the subsonic cases, and Schmidt et al.[5] showed that the two sides of peak is associated with downstream-traveling duct-like modes and upstream traveling discrete freestream modes, respectively.

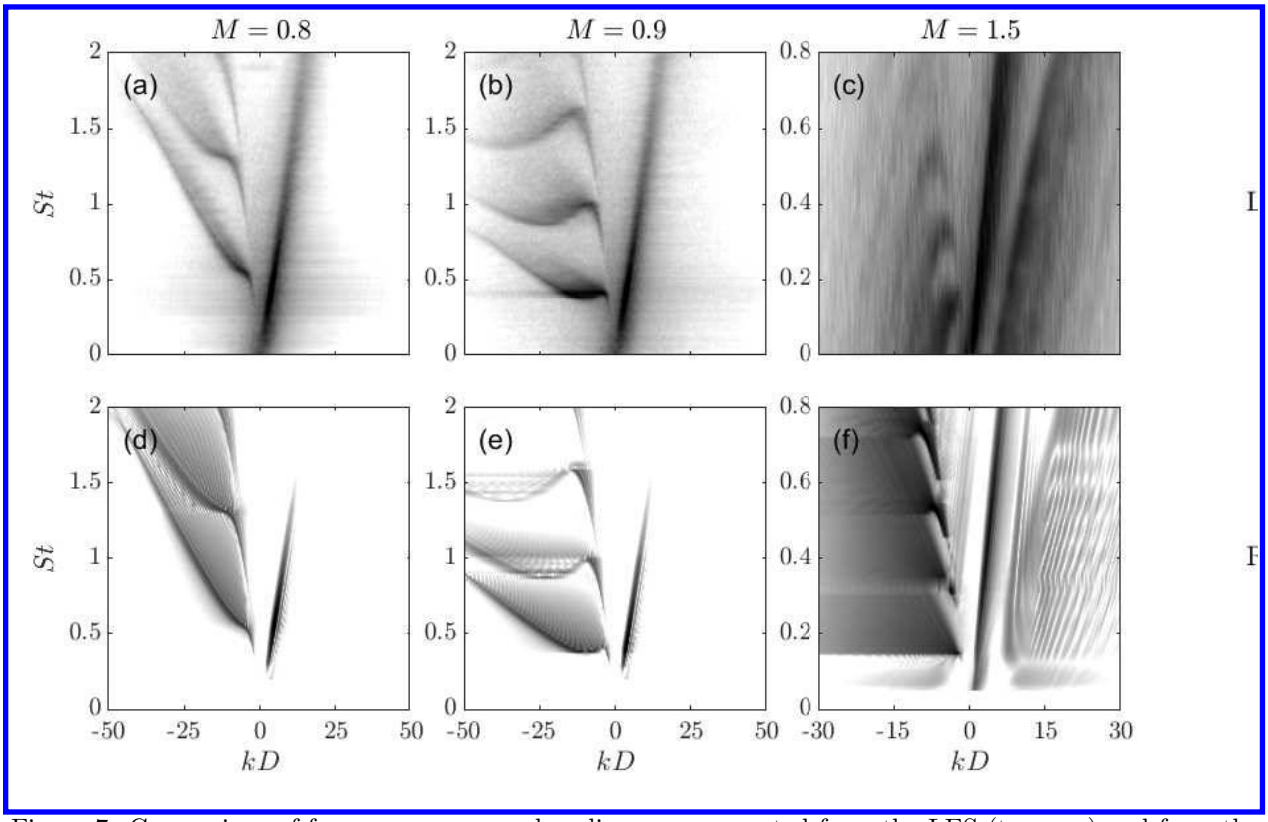

Figure 7: Comparison of frequency-wavenumber diagrams computed from the LES (top row) and from the revolvent model (bottom row) for: (a,d) $M = 0.8$; (b,e) $M = 0.9$; (c,f) $M = 1.5$. The contours levels are logarithmically and span four order of magnitude.

IV.C. Resolvent-approximated power spectra

Finally, we examine the resolvent-based low-rank approximations of the power spectral density of the centerline pressure. Figure 7 shows the frequency-wavenumber diagrams produced from the data and from the resolvent modes for $M = 0.8$, 0.9, and 1.5. As before, the results at each Mach number are normalized by the maximum amplitude along the Kelvin-Helmholtz dispersion relation, and the contours are logarithmically spaced and span four orders of magnitude. The agreement for the two subsonic jets is excellent – the model accurately captures the locations and changing shapes of the dispersion relations for the trapped waves. For the supersonic jet, the model qualitatively captures the basic shape and locations of the dispersion relations, but the results are not as crisp. This can likely be attributed to the lack of discrete modes in this case, which make the low-rank resolvent approximation more accurate for the subsonic jets.

Figure 8 shows the wavenumber filtered power spectra in $x - St$ space. The scaling of the results is the same as for Figure 5, but here we use linearly spaced contours to focus on the highest energy regions. As expected from the agreement in Figure 7, the model matches well with the LES data for the subsonic jets. In particular, the streamwise location of the resonating waves is well-captured. The agreement is not as good in the supersonic case, but the model does capture the approximate frequencies of the high-energy bands as well as their downstream position compared to the subsonic cases.

V. Conclusions

Previous models[3,4] have suggested that trapped acoustic waves inside the potential core of turbulent jets exhibit different behaviors within different Mach number regimes. In this work, we have provided evidence in support of these model predictions using data from large-eddy simulations of jets at five different Mach numbers. We demonstrate that the resonance observed at Mach 0.9 does not immediately vanish at the critical Mach number of 0.82, but instead slowly fades away as the Mach number is reduced.

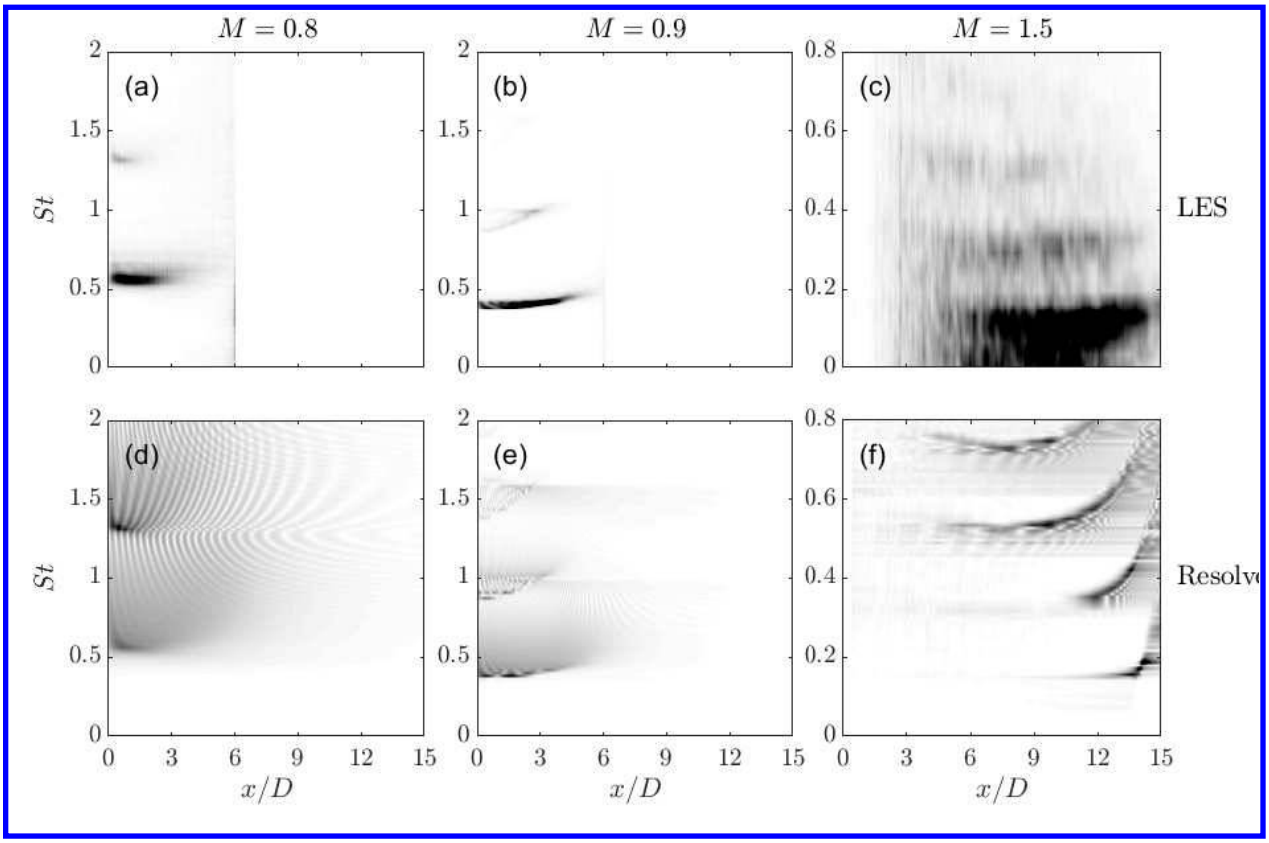

Figure 8: Comparison of filtered power spectral density computed from the LES (top row) and from the revolvent model (bottom row) for: (a,d) $M = 0.8$; (b,e) $M = 0.9$; (c,f) $M = 1.5$.

These behaviors were captured using global models based on the Navier-Stokes equations linearized about the turbulent mean flow. The global spectra showed that the discrete eigenvalues that describe the resonance do not vanish for Mach numbers below 0.82, but are instead increasingly damped. For supersonic Mach numbers, the discrete modes vanish, leaving only a continuous spectrum that exhibits peaks in the vicinity of the supersonic saddle point. Finally, we introduced a new global model based on resolvent analysis. This model shows that the above changes in the global spectrum as a function of Mach number account for the changes observed in the LES data.

Acknowledgments

The LES study was supported by NAVAIR SBIR project, under the supervision of Dr. John T. Spyropoulos. The main LES calculations were carried out on CRAY XE6 machines at DoD HPC facilities in ERDC DSRC.

References

[1]Jordan, P. and Colonius, T., "Wave Packets and Turbulent Jet Noise," *Annu. Rev. of Fluid Mech.*, Vol. 45, 2013, pp. 173–195.

[2]Michalke, A., "A Note on the Saptial Jet-instability of the Compressible Cylindrical Wortex Sheet," *Zentralstelle für Luftfahrtdokumentation und-information*, 1970.

[3]Tam, C. K. W. and Hu, F. Q., "On the three families of instability waves of high-speed jets," *J. Fluid Mech.*, Vol. 201, 1989, pp. 447–483.

[4]Towne, A., Cavalieri, A. V. G., Jordan, P., Colonius, T., Schmidt, O. T., Jaunet, V., and Brès, G. A., "Acoustic resonance in the potential core of subsonic jets," *J. Fluid Mech.*, Vol. 825, 2017, pp. 1113–1152.

[5]Schmidt, O. T., Towne, A., Colonius, T., Cavalieri, A. V. G., Jordan, P., and Brès, G. A., "Wavepackets and trapped acoustic modes in a turbulent jet: coherent structure eduction and global stability," *J. Fluid Mech.*, Vol. 825, 2017, pp. 1153–1181.

[6]Jordan, P., Jaunet, V., Towne, A., Cavalieri, A. V. G., Colonius, T., Schmidt, O. T., and Agarwal, A., "Jet–flap interaction tones," *J. Fluid Mech.*, Vol. 853, 2018, pp. 333–358.

[7]Gojon, R., Bogey, C., and Mihaescu, M., "Oscillation Modes in Screeching Jets," *AIAA J.*, 2018, pp. 1–7.

[8]Edgington-Mitchell, D., Jaunet, V., Jordan, P., Towne, A., Soria, J., and Honnery, D., "Upstream-travelling acoustic jet modes as a closure mechanism for screech," *J. Fluid Mech.*, Vol. 855, 2018.

[9]Edgington-Mitchell, D., Duke, D., Harris, D., Wang, T., Schmidt, O. T., Juanet, V., Jordan, P., and Towne, A., "Modulation of downstream-propagating waves in jet screech," *25th AIAA/CEAS Aeroacoustics Conference*, 2019.

[10]Shen, H. and Tam, C. K. W., "Three-dimensional numerical simulation of the jet screech phenomenon," *AIAA J.*, Vol. 40, No. 1, 2002, pp. 33–41.

[11]Mancinelli, M., Jaunet, V., Jordan, P., and Towne, A., "Screech-tone prediction for axisymmetric modes in supersonic jets using upstream-travelling acoustic jet waves," *(in prep.)*, 2018.

[12]Mancinelli, M., Jaunet, V., Jordan, P., Towne, A., and Girard, S., "Reflection coefficients and screech-tone prediction in supersonic jets," *25th AIAA/CEAS Aeroacoustics Conference*, 2019.

[13]Tam, C. K. W. and Ahuja, K. K., "Theoretical model of discrete tone generation by impinging jets," *J. Fluid Mech.*, Vol. 214, 1990, pp. 67–87.

[14]Bogey, C. and Gojon, R., "Feedback loop and upwind-propagating waves in ideally expanded supersonic impinging round jets," *J. Fluid Mech.*, Vol. 823, 2017, pp. 562–591.

[15]Jaunet, V., Mancinelli, M., Jordan, P., Towne, A., Edgington-Mitchell, D., Lehnasch, G., and Girard, S., "Dynamics of round jet impingement," *Proceedings of the 25th AIAA/CEAS Aeroacoustics Conference*, Amsterdam, Netherlands, 2019.

[16]Lessen, M., Fox, J. A., and Zien, H. M., "The instability of inviscid jets and wakes in compressible fluid," *J. Fluid Mech.*, Vol. 21, 1965, pp. 129–143.

[17]Brès, G. A., Ham, F. E., Nichols, J. W., and Lele, S. K., "Unstructured large-eddy simulations of supersonic jets," *AIAA J.*, 2017, pp. 1164–1184.

[18]Brès, G. A., Jordan, P., Jaunet, V., Le Rallic, M., Cavalieri, A. V. G., Towne, A., Lele, S. K., Colonius, T., and Schmidt, O. T., "Importance of the nozzle-exit boundary-layer state in subsonic turbulent jets," *J. Fluid Mech.*, Vol. 851, 2018, pp. 83–124.

[19]Kawai, S. and Larsson, J., "Wall-modeling in large eddy simulation: Length scales, grid resolution, and accuracy," *Phys. Fluids*, Vol. 24, 2012.

[20]Freund, J. B., "Proposed Inflow/Outflow Boundary Condition for Direct Computation of Aerodynamic Sound," *AIAA J.*, Vol. 35, No. 4, 1997, pp. 740–742.

[21]Mani, A., "Analysis and optimization of numerical sponge layers as a nonreflective boundary treatment," *J. Comput. Phys.*, Vol. 231, 2012, pp. 704–7016.

[22]Schmidt, O. T., Towne, A., Rigas, G., Colonius, T., and Brès, G. A., "Spectral analysis of jet turbulence," *J. Fluid Mech.*, Vol. 855, 2018, pp. 953–982.

[23]Towne, A., Schmidt, O. T., and Colonius, T., "Spectral proper orthogonal decomposition and its relationship to dynamic mode decomposition and resolvent analysis," *J. Fluid Mech.*, Vol. 847, 2018, pp. 821–867.

[24]Towne, A., Brès, G. A., and Lele, S. K., "A statistical jet-noise model based on the resolvent framework," *23rd AIAA/CEAS Aeroacoustics Conference, AIAA paper 2017-3706*, 2017.